ADVANCED ELECTRONIC MATERIALS
www.advelectronicmat.de

A Highly Sensitive Flexible Capacitive Tactile Sensor with Sparse and High-Aspect-Ratio Microstructures

*Yongbiao Wan, Zhiguang Qiu, Ying Hong, Yan Wang, Jianming Zhang, Qingxian Liu, Zhigang Wu, and Chuan Fei Guo**

Highly sensitive flexible tactile sensors that can be fabricated in a low cost and efficient way are in great demand for intelligent soft robotics and friendly human–machine interaction. Herein, a highly sensitive flexible tactile sensor is developed by using bionic micropatterned polydimethylsiloxane (m-PDMS) replicated from lotus leaf. The m-PDMS substrate consists of high-aspect-ratio and low-density microtowers, and is covered by ultrathin silver nanowires as a bottom electrode. The capacitive sensing device is constructed by sandwiching the bottom electrode, a colorless polyimides dielectric layer, and a top electrode, and exhibits a high sensitivity of ≈1.2 k Pa^{-1}, a ultralow limit of detection <0.8 Pa, and a fast response time of 36 ms. The finite-elemental analysis indicates that the sparse and high-aspect-ratio microtowers are critical to achieve high sensitivity, low limit of detection, and fast response to external stimulus. The flexible tactile sensor also exhibits high robustness: it can be tested for at least 100 000 cycles without showing fatigue. More importantly, the flexible tactile sensors are potentially useful in intelligent soft robots, health monitoring, and motion detection. Besides, the fabrication strategy may offer a guideline to design other microstructures for improving the performance of flexible tactile sensors.

1. Introduction

The rapid development in flexible tactile sensors has drawn a great deal of attention due to their wide applications in wearable electronics, human motion monitoring, personal healthcare, and artificial intelligence.[1–6] The artificial flexible tactile sensor converts external physical stimuli to recordable or measurable electrical signals.[5] The key parameters that evaluate flexible tactile sensors include sensitivity, response speed, limit of detection (LOD), and reliability. In recent years, various approaches have been investigated to fabricate tactile sensors and improve their performance. There are typically four types of sensing mechanisms for realizing tactile sensors, including piezoresistive,[7–9] capacitive,[10–13] piezoelectric,[14,15] and triboelectric types.[16,17] Capacitive tactile sensors utilize capacitance changes upon external pressure, presenting advantages of simple device construction, fast responding speed, low power consumption, and compact circuit layout, and are thereby widely investigated.[2,18–20]

A capacitive tactile sensor typically consists of two parallel plates that sandwich a dielectric layer. The capacitance (C) of a capacitor is determined by the effective area of two electrodes (A), the distance between plate electrodes (d), and the permittivity of dielectric layer (ε),[5] expressed as

$$C \propto A\varepsilon/d \tag{1}$$

For a flexible tactile sensor, the electrodes and the dielectric layer are required to be flexible. As an external force is applied on a flexible tactile sensor, the changes in A, d, and ε result in capacitance variations. Therefore, both flexible electrode and dielectric layer are crucial to determine the performance of tactile sensors. Conventional flexible electrodes are often obtained by coating conductors on flexible substrate or introducing conductive materials into polymer matrix.[4] Common substrates such as polydimethylsiloxane (PDMS), and popular conductive materials including graphene,[1] carbon nanotube,[21] metal nanowires,[22] and metal nanofilms,[11] have been widely used for flexible electrodes in tactile sensing. As for dielectric layer, flexible polymer materials such as polyvinylidene fluoride,[23] methyl methacrylate,[24] and Ecoflex silicone elastomers[25] are usually applied. However, the flexible tactile sensor based on parallel-plate capacitor is not sensitive owing to the small change in distance between narrow plane electrodes and the poor adhesion between the conductive layer and the flexible substrate.

According to Equation (1), changing any value of A, d, or ε will lead to the change of capacity. The sensitivity of a capacitive tactile sensor is highly related to the mechanical properties of the

Y. Wan, Z. Qiu, Y. Hong, Y. Wang, Prof. J. Zhang, Q. Liu, Prof. Z. Wu, Prof. C. F. Guo
Department of Materials Science and Engineering
Southern University of Science and Technology
Shenzhen 518055, China
E-mail: guocf@sustc.edu.cn

Y. Wan, Y. Hong, Y. Wang
School of Materials Science and Engineering
Harbin Institute of Technology
Harbin 150001, China

Prof. Z. Wu
State Key Laboratory of Digital Manufacturing Equipment and Technology
Huazhong University of Science and Technology
Wuhan 430074, China

The ORCID identification number(s) for the author(s) of this article can be found under https://doi.org/10.1002/aelm.201700586.

DOI: 10.1002/aelm.201700586

dielectric layer. An ideal dielectric layer should be as soft as possible so that d will be highly sensitive to external pressures. However, commonly used dielectric elastomers such as PDMS have a Young's modulus on MPa order, which may not have a perceptible deformation when loaded with a pressure of a few Pascal. While some elastomers are softer, they suffer from the high viscosity, which leads to slow response. In addition, thin PDMS film of a few micrometers in thickness exhibits obvious viscoelasticity.[23] An effective approach toward realizing highly sensitivity and fast response is to fabricate micropatterned structures of a low viscous material as the dielectric. Bao and co-workers used pyramid arrays as microstructured rubber dielectric layer to develop a highly sensitive flexible capacitive tactile sensor.[26] Park and co-workers also fabricated a high-performance capacitive sensor based on the micropatterned pyramidal ionic gels as the dielectric layer.[12] Note that the aforesaid micropatterns are molded with the silicon template obtained by using traditional lithography process with expensive instruments. Therefore, scientists are still looking for simpler and more cost-effective ways to make micropatterns. For instance, Wang et al. demonstrated a flexible tactile sensor based on the carbon nanotube and micropatterned PDMS (m-PDMS) molded from textile silk.[27] Shuai and co-workers reported a low-cost flexible capacitive tactile sensor based on prestrain-induced multiscale structures.[23] Kim et al. used a simple breath figures method to make microstructures with superhydrophobic nanoneedle arrays.[28] Lee and co-workers developed a capacitive pressure sensor based on the inartificial design of the surface roughness of paper.[29] More interestingly, many researchers used the natural materials as templates, such as rose petals, *E. aureum* leaves, and banana leaves, etc.,[8,30,31] to fabricate sensitive flexible tactile sensors. Compared with other unconventional methods, natural materials are easily available, environmental friendly, and are even more cost effective.

Two ways might be useful to further increase the sensitivity and low down the response time. First, microstructures with a higher aspect ratio are easier to destabilize and have more room to be compressed. Second, reducing the density of the microstructure can further make the dielectric layer "softer," and thus improve the sensitivity. Lotus leaf is a natural material that possesses superhydrophobicity and self-cleaning properties,[32] due to the unique microstructures of the microtower arrays on leaf surface as well as the extensive villi on the microtowers. The microstructures have a high aspect ratio and low density, such that they might be an ideal selection for high sensitive and fast response tactile sensors. Zhang and co-workers have successfully used the lotus leaf to fabricate complementary hole array for the electrode and self-assembled polystyrene (PS) microspheres as the dielectric layer in flexible tactile sensors with a sensitivity of 0.815 k Pa^{-1}.[11] However, the improved sensitivity originates from the PS sphere arrays, while the unique high aspect ratio and sparse microstructure of the lotus leaf has not yet be fully utilized.

Herein, we demonstrate an efficient strategy to fabricate highly sensitive flexible capacitive tactile sensor by using lotus leaf as the template. After two replications, m-PDMS with high-aspect-ratio (aspect ratio ≈ 2) and low-density microtower patterns was prepared for flexible substrate. To make the substrate conductive, ultrathin silver nanowires (AgNWs) with an average diameter of 20 nm were coated onto the m-PDMS film and uniformly comply with the shape of the microtowers. Colorless polyimide (CPI) with one-side-coated AgNWs was employed for dielectric layer as well as top electrode. By packaging the bottom electrode, dielectric layer, and top electrode, we obtained flexible capacitive tactile sensors with a high sensitivity up to 1.194 k Pa^{-1}, a fast response time of 36 ms, a low LOD of <0.8 Pa, and can be cycled for at least 100 000 times. We also demonstrate that the flexible tactile sensor is capable of detecting gas flow, and human motion such as finger, wrist, and elbow bending, which may enable applications in motion detection, health monitoring, and intelligent robots.

2. Results and Discussions

Figure 1a illustrates the fabrication process and device structure of the flexible capacitive tactile sensor. The replication process of the microstructured bottom electrode is based on a replica-molding method, which is a type of soft-lithography. After the first molding of the original template, the molded pattern is replicated again to create the microtowers array. For better quality of replication, hard PDMS (with a weight ratio of base to curing agent of 5:1), which has a larger Young's modulus than standard PDMS (base to curing agent ratio 10:1), was utilized, and such hard PDMS is suitable for replicating nanoscale patterns.[33] After the lotus surface is templated, an AgNW film was coated on the m-PDMS substrate. The top electrode was fabricated by coating AgNWs onto the top side of the CPI dielectric layer followed by coating a thin protective layer. Finally, the top electrode was laminated onto the micropatterned bottom electrode with the naked CPI surface facing the micropatterns, forming a sandwich structure.

Figure 1b shows a photo image of a fresh lotus leaf. After the first templating, uniform microcave arrays are obtained as shown in the scanning electron microscopy (SEM) image of Figure 1c. The average diameter of the caves is about 6.4 μm via random statistical distribution (see Figure S1a, Supporting Information). After fluorination treatment and second templating, uniform microtowers of PDMS with an average diameter of ≈6.5 μm and height of ≈14 μm (Figure S1b,c, Supporting Information) were replicated as shown in Figure 1d–f. It can be found that the microtowers are sparsely distributed. The as-fabricated m-PDMS film (Figure 1g) is not transparent due to the light scattering caused by the microstructures. Significantly, a second molding template can be reused for several times and the m-PDMS films in different cycles of templating can still maintain the morphology and features, as shown in Figure S2 in the Supporting Information. It is worth noting that there is a curl of the lotus leaf itself. To eliminate the defects in lotus leaf, we cut a rectangle on centimeter scale along the edge keeping away from the veins of the lotus leaf, and place it on a horizontal desktop pasted by 3M tap. After two replicas, we were able to get flat and microstructured PDMS films. In addition, decreasing the sample size is helpful to avoid a curl.

The fabrication of the micropatterned bottom electrode is critical for sensing device. As described in previous reports,[34] coating metal nanofilm onto the flexible substrate is a general approach to obtain the flexible electrode. However, cracks might be formed after cyclic stretches or compressions, thus

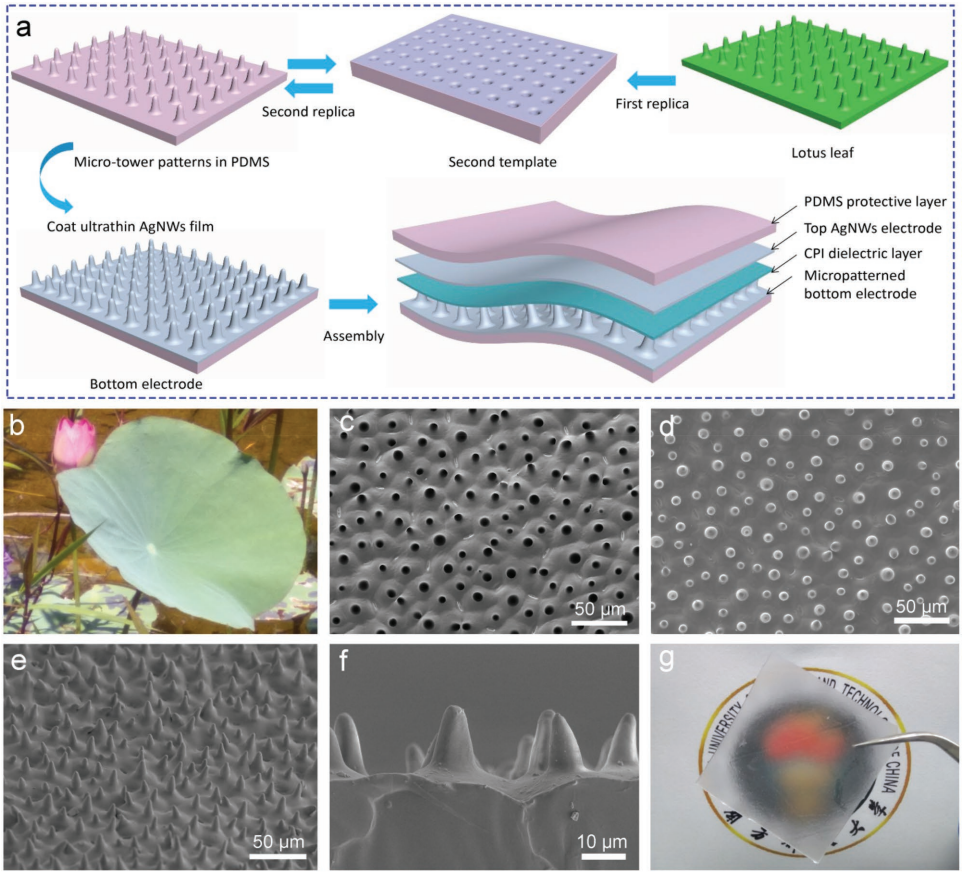

Figure 1. Fabrication of the m-PDMS and flexible tactile sensors. a) Schematic illustration for the fabrication of micropatterned tactile sensor. b) The photo image of a lotus leaf. c,d) The top view SEM images of the second molding template and the m-PDMS via two replicas, respectively. e) 45° tilt view SEM image of the m-PDMS. f) The cross-sectional view SEM image of the PDMS microtowers. g) Photo image of as-fabricated m-PDMS, showing haze caused by the microtowers.

leading to a degeneration of the conductivity of flexible electrode. In this work, we choose ultrathin AgNWs as the conductive layer on the m-PDMS. As displayed in **Figure 2**a, the SEM and transmission electron microscopy (TEM) images show that the AgNWs have a small diameter of about 20 nm and a typical length of larger than 30 μm. After coating, the ultrathin AgNWs film well complies with the microtowers array as shown in Figure 2b, and a magnified SEM (Figure 2c) shows that the AgNWs are uniformly distributed on the microtower and other areas. In the coating process, the dimensions of AgNWs play a critical role to achieve uniform distribution. The buckling force (F_b) of AgNWs is given by the Euler equation[35,36]

$$F_b = 192\,EI\Delta Z_{center}/L^3 \tag{2}$$

where ΔZ_{center} is the resulting displacement of the beam at the load point, E, I and L are the elastic modulus, the moment of inertia, and the length of AgNWs, respectively. For a cylindrical AgNW, I is given by the following equation

$$I = \pi D^4/64 \tag{3}$$

where D is the diameter of AgNWs. According to Equations (2) and (3), the buckling force dramatically decreases with the decreasing diameter and increasing length. Therefore, our ultrathin AgNWs (only ≈20 nm in diameter but with a large length of ≈30 μm) will exhibit quite poor flexural rigidity and good compliance. When coated on m-PDMS, the ultrathin AgNWs could be easily compliant with the shape of the microtowers driven by capillary force,[37] and the film exhibits a low sheet resistance (R_{sq}) below 10 $\Omega\cdot sq^{-1}$. In comparison, we have also coated coarser AgNWs with a diameter of 50 nm and a smaller length <20 μm on the m-PDMS under the same condition (see Figure S3, Supporting Information). The coarser AgNWs did not uniformly cover on the microtowers due to the larger flexural rigidity, but fell on the bottom of microtowers (Figure S3, Supporting Information; and Figure 2e). Besides the bottom electrode, the top electrode was easily fabricated by simply coating dense ultrathin AgNWs with a sheet resistance below 10 $\Omega\cdot sq^{-1}$ onto the CPI dielectric layer (Figure S4, Supporting Information). A thin PDMS protective layer was then coated on top of the AgNWs film on CPI.

The sensing performance of the flexible capacitive tactile sensor is evaluated in **Figure 3**. To investigate the effect of the microtower patterns in bottom electrode on the sensing performance, we have also fabricated a sensor in which a planar PDMS coated with AgNWs was used to replace the

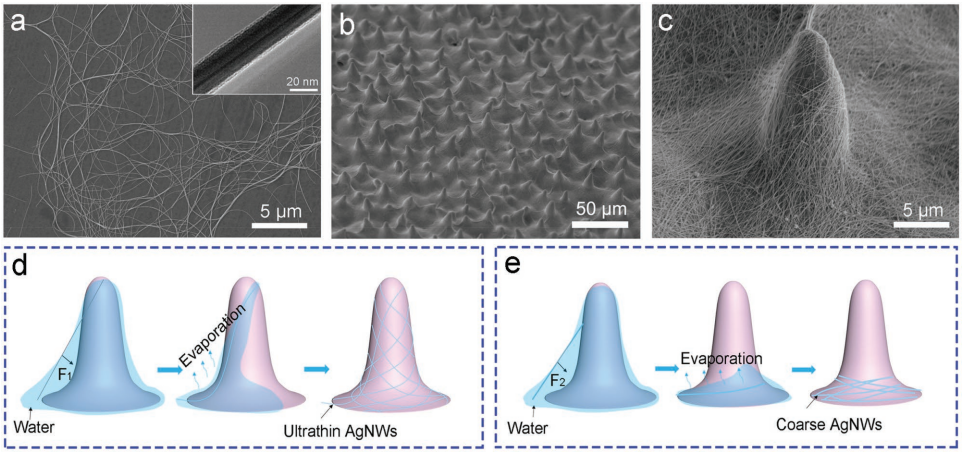

Figure 2. Ultrathin AgNWs and the shape-compliant property. a) Typical SEM and TEM (inset) Images of the ultrathin AgNWs with a diameter of ≈20 nm. b) The morphology of ultrathin AgNWs coated on m-PDMS. c) A detailed image of AgNWs on a microtower, indicating that the AgNWs well complies with the shape of the microtowers. Schematic illustrations of the ultrathin and coarse AgNWs coated on the microtowers. d) The ultrathin AgNWs with low flexural rigidity could easily bend and uniformly comply on the microtowers. e) The coarse AgNWs show a high flexural rigidity and thus fall on the bottom of microtowers when pulled by the capillary force.

micropatterned bottom electrode (Figure 3a) for comparison. The sensitivity is given by

$$S = \delta\left(\Delta C/C_0\right)/\delta P \tag{4}$$

where C_0 is the initial capacitance, ΔC is the relative change of capacitance (C–C_0), and P is the applied pressure. Based on the principle, we can evaluate the sensitivity of the sensor by depicting the tangent of the curve on pressure-dependent capacitance change rate and calculating the slop of the tangent. As shown in Figure 3b, two linear regions of capacitance change rate as a function of applied pressure were observed. For the micropatterned sensor, when the applied pressure is higher than 2 kPa, the sensitivity of the device is 0.077 k Pa^{-1}; and in

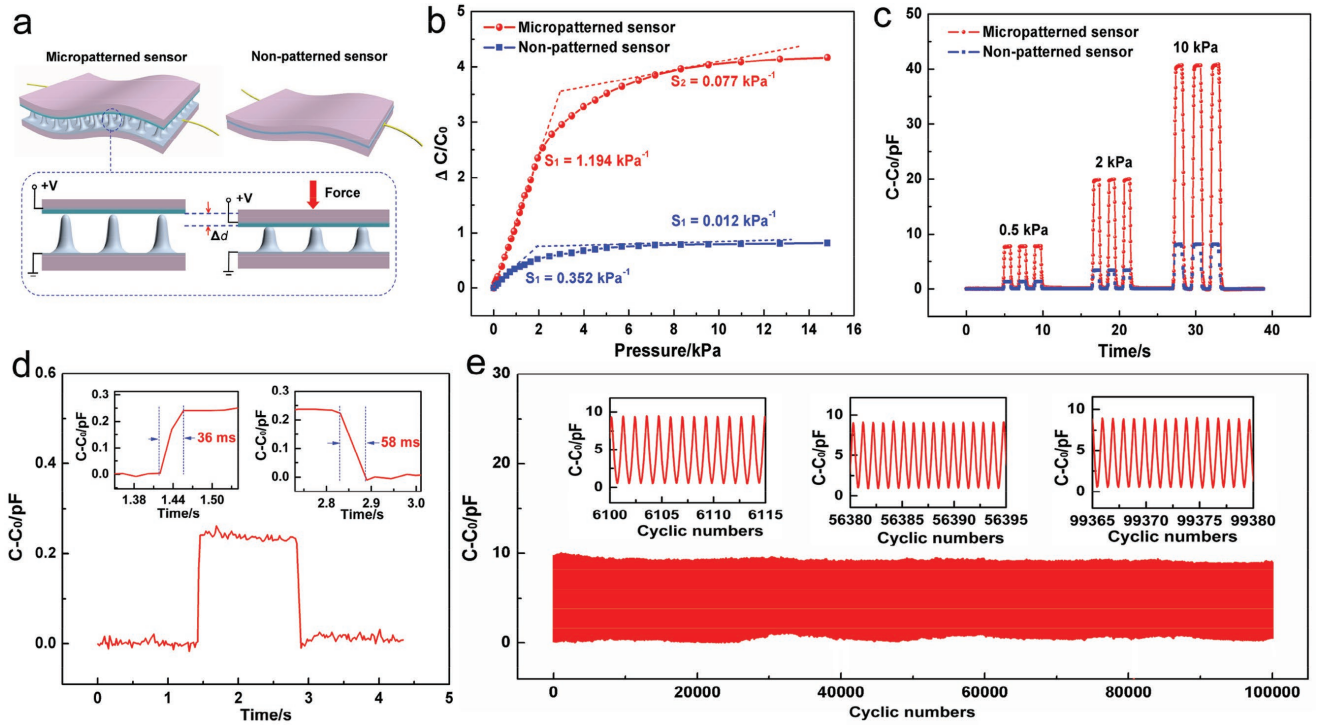

Figure 3. Properties of the tactile sensors. a) The schematics of the configuration of the micropatterned device and nonpatterned device, as well as the sensing mechanism of the micropatterned tactile sensor. b–e) Sensitivity, LOD, response time, and robustness of flexible tactile sensors: b) Sensitivity of the micropatterned (red circles) and nonpatterned sensor (blue squares). c) Repeated real-time responses to the pressure of 0.5, 2, and 10 kPa for the two types of sensors. d) Real-time response of the sensor to an ultralow pressure of 0.8 Pa. The insets show the response time upon loading and unloading. e) Stability of the sensor tested for 100 000 cycles under an applied pressure of 0.4 kPa, and the insets show signal under different number of cycles.

the pressure regime less than 2 kPa, the sensitivity of the device reaches 1.194 k Pa^{-1}. By contrast, the nonpatterned sensor shows much lower sensitivities of 0.012 and 0.352 k Pa^{-1} in the pressure regions higher and smaller than 2 kPa, respectively. To evaluate the repeatability of the sensors, we tested real-time responses of device with quick loading/unloading pressures of 0.2, 2, and 10 kPa for three circles each (Figure 3c). The results show that the micropatterned sensors present stable responses with a high sensitivity and great repeatability.

Furthermore, to investigate the LOD and response time of micropatterned tactile sensor, a piece of slight paper (20 mg or 0.8 Pa) was uniformly loaded on the entire surface of device, and the result is shown in Figure 3d. When loading with the slight paper, the capacitance of the sensor rapidly ascended within a fast response time of 36 ms, which is comparable to the response time of human skin (30–50 ms),[38] and then stayed at a stable value. After removing the slight paper, the capacitance of the sensor decreased promptly with a short recovery component in about 58 ms, and thereafter attenuated to its initial value (see the inset of Figure 3d). The difference in the response time for loading and unloading might be ascribed to that unloading is slower than loading. We have also tested the robustness of the flexible tactile sensor, by repeatedly loading/unloading a pressure pulse (0.4 kPa) for 100 000 times, and it shows that the device well maintains its function without showing obvious fatigue (Figure 3e). The insets in Figure 3e show signals under three different stages of repeated test, exhibiting quite similar waveforms, and the results indicate that during the 100 000 cycles of loading/unloading, no fatigue appears. In comparison to the reported results in literature (see Table S1 in the Supporting Information for a summary of flexible capacitive tactile sensors reported elsewhere), our micropatterned sensor exhibits high comprehensive performances in high sensitivity, low LOD, and good stability and reliability, although not the best in all aspect.

The bionic microstructures and ultrathin AgNWs play important roles to the high performance of the sensors. First, the microstructures can deform more easily than solid dielectric films and this leads to higher sensitivity. In the sensor structure, dielectric layer consists of the CPI film together with the air gaps between the CPI film and microstructured electrodes. Figure S5 in the Supporting Information shows the deformation of bionic microstructures upon pressing. In principle, the thickness of the CPI film will not be significantly changed due to the higher Young' modulus (3.5 GPa), and the change in d largely comes from the deformation of the microtowers or the change in thickness of the air gap. In order to understand the mechanism of the effect of bionic microstructures on sensing performance, finite-elemental analysis (FEA) simulating the deformation of two CPI film/PDMS microtowers/PDMS structures with different tower densities against increasing external pressure was conducted, and a CPI/PDMS bilayer with the same thickness was used for comparison, as shown in **Figure 4**. The details of the FEA simulation are described in the Experimental Section and Figure S6 in the Supporting Information, and the model was up-scaled for 1000 times. A sparse (0.263 cm^{-2}, Figure 4a) and a dense (0.591 cm^{-2}, Figure 4b) microtowers array, and a thin PDMS layer (Figure 4c) with the same thickness (14 mm) are compared regarding the maximum contact stress in PDMS (Figure 4d) as well as the change in height (Figure 4e) under different pressures of 0.5, 2, and 10 kPa. When a pressure is applied to the structures, local stress is concentrated at the contact points between the microtowers array and CPI dielectric layer. Compared with a continuous and nonpatterned PDMS layer, the microtowers array exhibits much larger local stresses. Moreover, the ratio of $\Delta d/d$ (change in height) for microstructured PDMS is tens of times higher than that in continuous PDMS. Especially for the sparse microtowers, $\Delta d/d$ is even about twice that of the dense microtowers, approximately inversing to the density of towers, and approximately twenty times higher than that of continuous PDMS. The simulation illustrates two principles: first, the change in height for micropattern PDMS is much more sensitive to external pressure than that in a continuous PDMS film; second, decreasing the density of microtowers is helpful to further achieve a large change in height. Although the effect of the AgNWs has not been considered in the simulation, we can still conclude that sparse microstructures are desired in device design. Bao and co-workers have first developed the micropyramidal PDMS-based capacitive pressure sensor with a similar mechanism.[26] The micropyramids only show a height-to-width aspect ratio of 0.5, while our microtowers have a much larger aspect ratio of over 2. In addition, the distance between our microtowers is about 20 μm, much wider than 5 μm for the micropyramids in Bao's paper. All of these features of our microstructures would cause easier change in the height of dielectric (d) and thus contribute positively to LOD and sensitivity.

Second, the bionic microstructures show a faster response than a thin viscoelastic PDMS layer or other elastomers with a lower elastic modulus (e.g., Ecoflex). In order to improve sensitivity of tactile sensors, dielectric layers with a low Young's modulus are often applied.[2] However, softer dielectrics often show higher viscosity, and PDMS with a small thickness also shows increased viscosity,[23] which results in a lower response speed, so that soft and highly viscous dielectrics should be avoided. In this work, the PDMS microtowers allow for easier deformation while keeping fast response speed.

Third, the ultrathin AgNW film exhibits significant advantages over common metal films. The AgNWs used in this work have a diameter of ≈20 nm and a length-to-diameter aspect ratio over 1000, enabling compliant coating on microstructured surfaces and high electrical conductance. Moreover, AgNW films have proven to be highly flexible or even stretchable.[37]

A few demonstrations of application of the tactile sensors are shown in **Figure 5**. The simple response of the sensor to normal pressing is shown in Figure 5a. The tactile sensor could immediately response to repeated finger touching. In addition, our device could also accurately respond to different repeated dynamic flexion and straightening motions of the finger, wrist, and elbow while exhibiting reproducible response and relaxation behaviors at each cycle, as shown in Figure 5b–e. This clearly suggests that the flexible tactile sensor can be used as a skin-mountable wearable sensor-to-monitor human motion, or even be employed in artificial intelligence. Based on its superior sensing performance, the flexible sensor can be used to monitor subtle biomedical signals, such as breathing (Figure S7, Supporting Information). In addition to direct pressure, we have also investigated the real-time response of

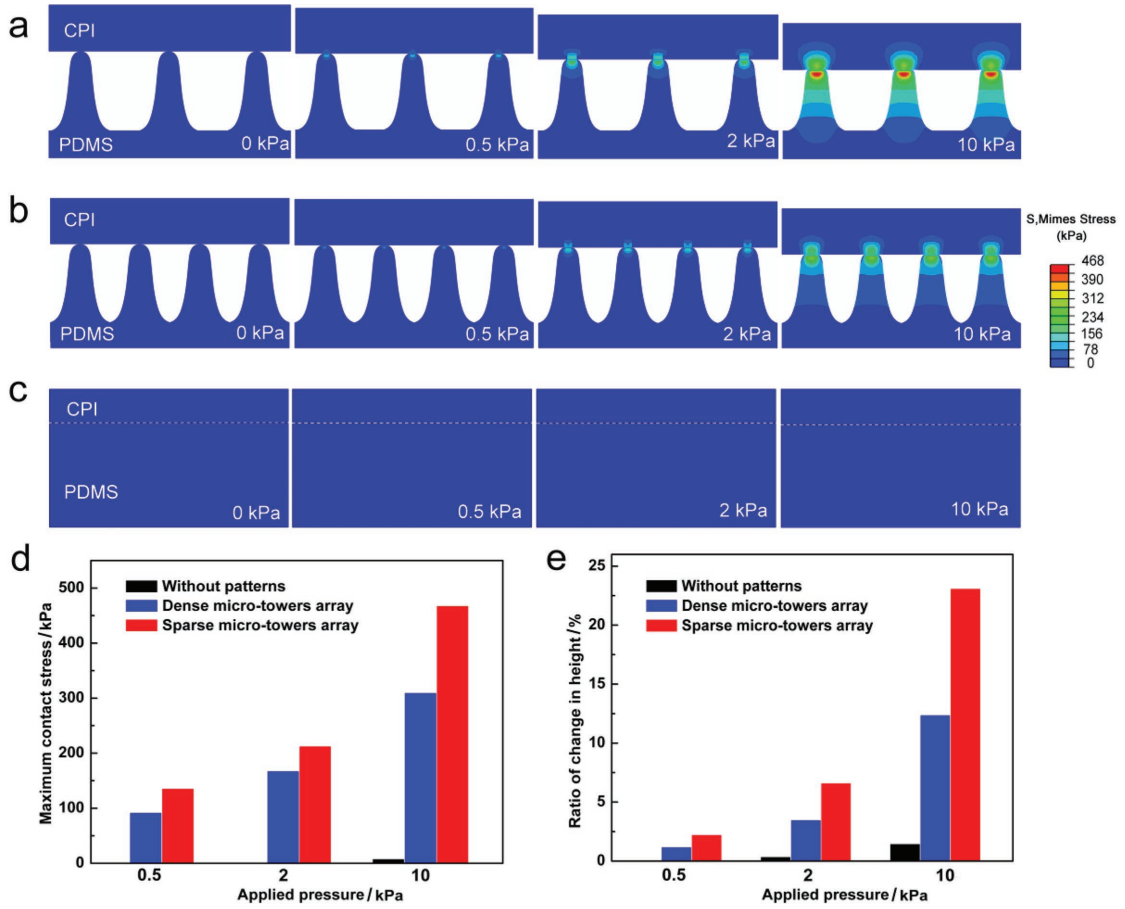

Figure 4. Finite-element simulation showing the local stress distribution and the deformation of a) sparse and b) dense microtowers array, and c) nonpatterned PDMS at pressures of 0.5, 2, and 10 kPa. ABAQUS was used for the simulation and the contact of the microtower arrays, and CPI dielectric layer was assumed to be frictionless. d) Simulated maximum contact stress and e) ratio of change in height of three structures under applied pressures of 0.5, 2, and 10 kPa.

the tactile sensor to the airflow (Figure 5f). A rubber suction bulb was used to generate airflow, and the real-time response signal was recorded. Remarkable peaks could be seen when the rubber suction bulb is gripped. During the test, airflow plays a role of medium for transmitting the pressure to the sensor without direct contact. The signal intensity corresponds to weak or strong airflows and can be used to monitor airflow for possible applications in atmospheric science and aerospace.

3. Conclusion

In this study, we have fabricated the high-performance flexible capacitive tactile sensor based on micropatterned elastomeric electrode by using a bio-inspired and low-cost approach. The micropatterned elastomeric electrode was prepared by coating the ultrathin AgNWs onto the m-PDMS with uniform microtower patterns replicated from the inexpensive lotus leaf molding template. The ultrathin AgNWs could be tightly cocooned around the microtower patterns and maintain the advantage of the patterns with high aspect ratio and low density. The capacitive sensor was constructed by sandwiching a micropatterned bottom electrode, a CPI dielectric layer, and a top electrode. The obtained flexible tactile sensor exhibits a sensitivity of 1.194 k Pa^{-1} (when applied pressure < 2 kPa), which is obviously higher than the nonpatterned sensors. Furthermore, the flexible sensor is featured with a low LOD below 0.8 Pa, a fast response time within 36 ms, while showing no fatigue after 100 000 cycles of touching. Such high performance enables the flexible tactile sensor to detect the touching sense, limb motions, heartbeat, and gas flow. Considering the unique properties of the device, we expect that our sensor could offer promising potential for applications in smart electronics and artificial intelligence.

4. Experimental Section

Materials: Ethylene glycol (EG, AR), poly(vinylpyrrolidone) (PVP) (average M_w of 360 000), silver nitrate ($AgNO_3$, 99.8%), sodium chloride (NaCl, 99.8%), and potassium bromide (KBr, 99.8%) were all purchased from Sigma-Aldrich (St. Louis, MO). Ethanol (99%) and acetone (98%) were acquired from Sinopharm Chemical Reagent Co., Ltd. All chemicals were used as received without further purification. Deionized water with a resistivity of 18.2 MΩ cm was used throughout the experiments. Thermal water kettle (volume: 100 mL) and CPI with a thickness of 15 µm were purchased from Shanghai Chemical Reagents Co., Ltd. The PDMS elastomer (Sylgard 184) was purchased from Dow Corning Co., Ltd.

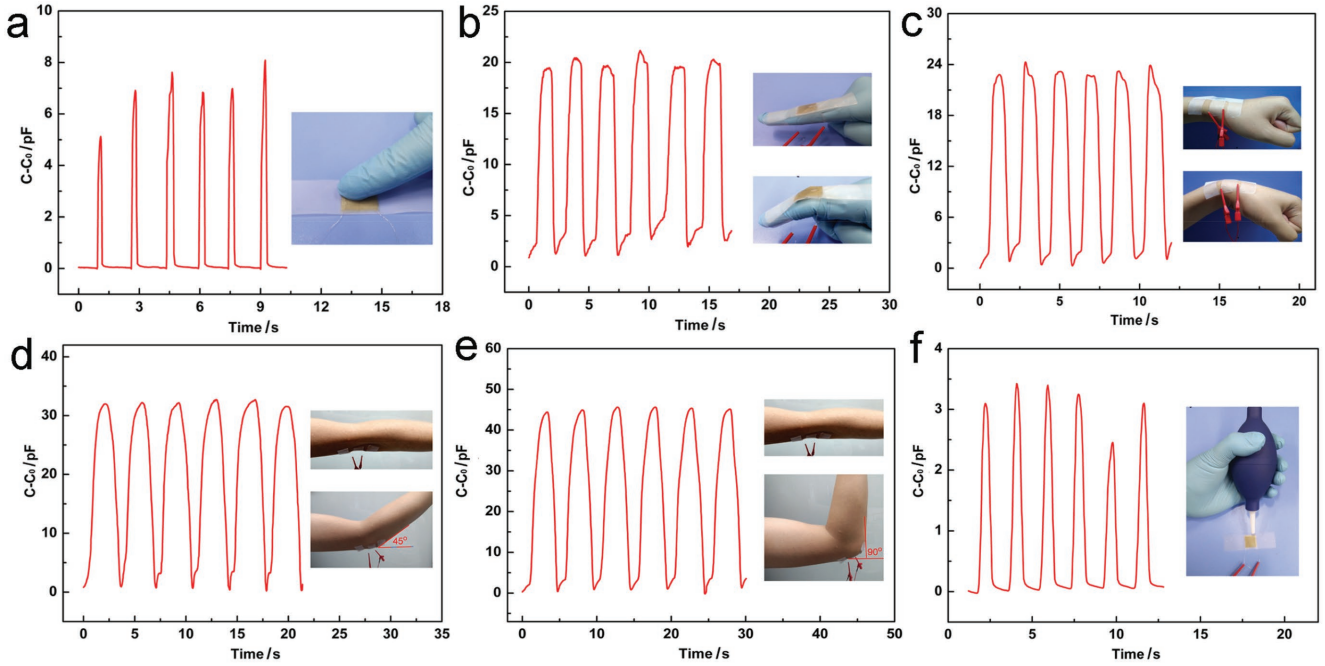

Figure 5. Real-time monitoring of capacitance changes upon pressing caused by repeated a) finger touching, b) finger bending, c) wrist bending, d,e) elbow bending with a 45° and a 90° angles, respectively, and f) airflow.

Synthesis of Ultrathin AgNWs: Ultrathin silver nanowires were synthesized as following: Fresh $AgNO_3$ solution (0.2255 g) was dissolved in EG (5 mL). PVP-360 000 (0.28 g), NaBr solution (0.0114 g), NaCl solution (0.0123 g), and EG (50 mL) were successively added into a flask (100 mL) placed in an oil bath at room temperature under magnetic stirring (300 rpm). Then the solution was slowly heated to 170 °C. Nitrogen gas (100 mL min^{-1}) was bubbled through the reaction during heating. Subsequently, the $AgNO_3$ solution (5 mL) was added through a syringe pump at an injection rate of 0.5 mL min^{-1}. The reaction mixture was held at 150 °C for 0.5 h without magnetic stirring and then quenched by immersing the flask in an ice-water bath for 30 min. The reaction product was washed with acetone three times to remove the extra solvent and chemical agents (PVP and other reactants). The prepared AgNWs were dispersed in ethanol.

Fabrication of Micropatterned Electrode: Fresh lotus leaf was cut into rectangular shapes and washed deionized water for three times. After dried by N_2 gas blowing, the lotus leaf was fixed on a glass substrate using Scotch tapes. For better quality of replication, PDMS with a base to curing agent ratio of 5:1 was prepared and placed at room temperature until bubbles disappeared. Then a certain amount of PDMS mixture was poured on the leaves. After curing at 70 °C for 1 h, the PDMS film with the inverse structures of lotus leaf was peeled off as a second molding template. To weaken adhesion during the second molding process, the molding template was treated by fluorination. The second molding process was similar to the first molding process except for utilization of standard PDMS (the weight ratio of base to crosslinker was 10:1). After the hard and standard PDMS double-layer molding process, a replica of the original surface, that is, the m-PDMS film with positive pattern of lotus leaf was fabricated. Next, ultrathin AgNWs were coated onto the m-PDMS. To enhance the adhesion between the AgNWs and m-PDMS substrate, the sample was treated at 70 °C for 30 min.

Preparation of Top Electrode, Dielectric Layer, and Tactile Sensor: The ultrathin AgNWs were coated on a CPI film by using a Mayer rod, and then dried at 70 °C for 10 min. Following that a silver wire was mounted on the terminal of AgNWs film, and a layer of uncured PDMS mixture was poured onto the AgNWs film and cured at 70 °C for 1 h forming a protective layer. Subsequently, the top electrode with a size of 1.5 × 1.5 cm^2 was laminated onto the same sized micropatterned bottom electrode with a CPI dielectric layer facing the micropatterns. Finally, the edges were bonded together using 3M Scotch tape to assemble the sandwich structured tactile sensor.

Characterization and Measurements: The microstructures of the samples were inspected by field-emission scanning electron microscopy (TESCAN) operated at 5 kV. The transmission electron microscopy (TEM) image was characterized using an FEI Tecnai F30 microscopy operated at 200 kV. The external pressure was applied using a force gauge with a computer-controlled stage (XLD-20E, Jingkong Mechanical testing Co., Ltd). The capacitance was measured using an inductance capacitance and resistance (LCR) meter (E4980AL, KEYSIGHT) with a testing frequency of ≈50 Hz. For cyclic loading/unloading tests, the sensor was placed on the testing system, and a preselected constant pressure was repeatedly applied and released while the electrical signals were recorded.

FEA: A 3D model and numerical simulations were performed using ABAQUS (V6.14-4, Dassault Systèmes). Because of the symmetry condition of the model, only one-fourth of the model was considered. The original height and diameter of microtowers were 14 and 6.5 mm, respectively. To simplify the simulation processes, the AgNWs film was ignored. The bionic microstructured PDMS and CPI layer were partitioned on each other, and the material properties such as density, Young's modulus, and Poisson's ratio (see Table S2, Supporting Information) were assigned at each section. The meshes with the C3D10 type were arranged radially, and finer meshes were used for the contact area in order to increase the numerical accuracy of the model. In the model, the whole nodes were 1234, and the total degrees of freedom were 1, 204, and 376. The supporting surface was selected by the m-PDMS film with the nonpatterned surface. A load was applied to the top of the CPI layer, and the applied load was gradually increased to 10 kPa. The contact condition of the microtowers was assumed to be frictionless. As the model is symmetrical in the longitudinal and transverse directions, symmetry boundary conditions were applied to the four cut planes. The change in height of microtower was captured after the loading of 10 kPa, showing that the displacement Δd in the vicinity of the contact region was 3.23 mm. Finally, the Quarter-symmetry tower model can be changed to a complete tower model by mirroring operation. After offsetting the whole microtower model, a rectangular pattern of microtower arrays can be gotten. For dense microtower

arrays, the distance between two microtowers is 13 mm. But for sparse microtower arrays, the distance between two microtowers is 19.5 mm.

Supporting Information

Supporting Information is available from the Wiley Online Library or from the author.

Acknowledgements

Y.W. and Z.Q. contributed equally to this work. This work was financially supported by the funds of the "Guangdong Innovative and Entrepreneurial Research Team Program" under contract No. 2016ZT06G587, the National Natural Science Foundation of China (No. U1613204), the "Science Technology and Innovation Committee of Shenzhen Municipality" (Grant No. JCYJ20160613160524999), and the "Peacock Plan" (No. Y01256120). The authors thank W. Zhou in Kingfa Science and Technology Co., Ltd. for the help on finite-element simulation.

Conflict of Interest

The authors declare no conflict of interest.

Keywords

fatigue, flexible tactile sensors, human motion detection, micropatterned PDMS, sensitivity

Received: November 27, 2017
Revised: December 26, 2017
Published online: March 1, 2018

[1] Y. Wang, L. Wang, T. T. Yang, X. Li, X. B. Zang, M. Zhu, K. L. Wang, D. H. Wu, H. W. Zhu, *Adv. Funct. Mater.* **2014**, *24*, 4666.
[2] M. L. Hammock, A. Chortos, B. C. K. Tee, J. B. H. Tok, Z. Bao, *Adv. Mater.* **2013**, *25*, 5997.
[3] Y. Zang, F. Zhang, C. Di, D. Zhu, *Mater. Horiz.* **2015**, *2*, 140.
[4] X. Wang, Z. Liu, T. Zhang, *Small* **2017**, *13*, 1602790.
[5] Y. Wan, Y. Wang, C. F. Guo, *Mater. Today Phys.* **2017**, *1*, 61.
[6] S. Gong, D. T. H. Lai, B. Su, K. J. Si, Z. Ma, L. W. Yap, P. Guo, W. Cheng, *Adv. Electron. Mater.* **2015**, *1*, 140063.
[7] J. Park, Y. Lee, J. Hong, M. Ha, Y. D. Jung, H. Lim, S. Y. Kim, H. Ko, *ACS Nano* **2014**, *8*, 4689.
[8] M. Jian, K. Xia, Q. Wang, Z. Yin, H. Wang, C. Wang, H. Xie, M. Zhang, Y. Zhang, *Adv. Funct. Mater.* **2017**, *27*, 1606066.
[9] Y. D. Li, Y. N. Li, M. Su, W. B. Li, Y. F. Li, H. Z. Li, X. Qian, X. Y. Zhang, F. Y. Li, Y. L. Song, *Adv. Electron. Mater.* **2017**, *3*, 1700253.
[10] D. J. Lipomi, M. Vosgueritchian, B. C. K. Tee, S. L. Hellstrom, J. A. Lee, C. H. Fox, Z. Bao, *Nat. Nanotechnol.* **2011**, *6*, 788.
[11] T. Li, H. Luo, L. Qin, X. Wang, Z. Xiong, H. Ding, Y. Gu, Z. Liu, T. Zhang, *Small* **2016**, *12*, 5042.
[12] S. H. Cho, S. W. Lee, S. Yu, H. Kim, S. Chang, D. Kang, I. Hwang, H. S. Kang, B. Jeong, E. H. Kim, S. M. Cho, K. L. Kim, H. Lee, W. Shim, C. Park, *ACS Appl. Mater. Interfaces* **2017**, *9*, 10128.
[13] S. Kang, J. Lee, S. Lee, S. Kim, J.-K. Kim, H. Algadi, S. Al-Sayari, D.-E. Kim, D. Kim, T. Lee, *Adv. Electron. Mater.* **2016**, *2*, 1600356.
[14] W. Wu, X. Wen, Z. L. Wang, *Science* **2013**, *340*, 952.
[15] Z. F. Chen, Z. Wang, X. M. Li, Y. X. Lin, N. Q. Luo, M. Z. Long, N. Zhao, J. B. Xu, *ACS Nano* **2017**, *11*, 4507.
[16] F.-R. Fan, L. Lin, G. Zhu, W. Wu, R. Zhang, Z. L. Wang, *Nano Lett.* **2012**, *12*, 3109.
[17] T. Li, J. Zou, F. Xing, M. Zhang, X. Cao, N. Wang, Z. L. Wang, *ACS Nano* **2017**, *11*, 3950.
[18] X. D. Wang, L. Dong, H. L. Zhang, R. M. Yu, C. F. Pan, Z. L. Wang, *Adv. Sci.* **2015**, *2*, 1500169.
[19] B. Q. Nie, R. Y. Li, J. Cao, J. D. Brandt, T. R. Pan, *Adv. Mater.* **2015**, *27*, 6055.
[20] S. Pyo, J. Choi, J. Kim, *Adv. Electron. Mater.* **2017**, *3*, 1700427.
[21] Y. Song, H. T. Chen, Z. M. Su, X. X. Chen, L. M. Miao, J. X. Zhang, X. L. Cheng, H. X. Zhang, *Small* **2017**, *13*, 1702091.
[22] Y. Heo, Y. Hwang, H. S. Jung, S. H. Choa, H. C. Ko, *Small* **2017**, *13*, 1700070.
[23] X. Shuai, P. Zhu, W. Zeng, Y. Hu, X. Liang, Y. Zhang, R. Sun, C.-P. Wong, *ACS Appl. Mater. Interfaces* **2017**, *9*, 26314.
[24] Y. Joo, J. Byun, N. Seong, J. Ha, H. Kim, S. Kim, T. Kim, H. Im, D. Kim, Y. Hong, *Nanoscale* **2015**, *7*, 6208.
[25] D. Kwon, T.-I. Lee, J. Shim, S. Ryu, M. S. Kim, S. Kim, T.-S. Kim, I. Park, *ACS Appl. Mater. Interfaces* **2016**, *8*, 16922.
[26] S. C. B. Mannsfeld, B. C. K. Tee, R. M. Stoltenberg, C. V. H. H. Chen, S. Barman, B. V. O. Muir, A. N. Sokolov, C. Reese, Z. Bao, *Nat. Mater.* **2010**, *9*, 859.
[27] X. Wang, Y. Gu, Z. Xiong, Z. Cui, T. Zhang, *Adv. Mater.* **2014**, *26*, 1336.
[28] J. Kim, B. Lew, W. S. Kim, *Nanoscale Res. Lett.* **2011**, *6*, 616.
[29] K. Lee, J. Lee, G. Kim, Y. Kim, S. Kang, S. Cho, S. Kim, J.-K. Kim, W. Lee, D.-E. Kim, S. Kang, D. Kim, T. Lee, W. Shim, *Small* **2017**, *13*, 1700368.
[30] Y. Wei, S. Chen, Y. Lin, Z. Yang, L. Liu, *J. Mater. Chem. C* **2015**, *3*, 9594.
[31] P. Nie, R. Wang, X. Xu, Y. Cheng, X. Wang, L. Shi, J. Sun, *ACS Appl. Mater. Interfaces* **2017**, *9*, 14911.
[32] L. Feng, S. H. Li, Y. S. Li, H. J. Li, L. J. Zhang, J. Zhai, Y. L. Song, B. Q. Liu, L. Jiang, D. B. Zhu, *Adv. Mater.* **2002**, *14*, 1857.
[33] D. Qin, Y. N. Xia, G. M. Whitesides, *Nat. Protoc.* **2010**, *5*, 491.
[34] I. M. Graz, D. P. J. Cotton, S. P. Lacour, *Appl. Phys. Lett.* **2009**, *94*, 071902.
[35] A. Heidelberg, L. T. Ngo, B. Wu, M. A. Phillips, S. Sharma, T. I. Kamins, J. E. Sader, J. J. Boland, *Nano Lett.* **2006**, *6*, 1101.
[36] K. Inaba, K. Saida, P. Ghosh, K. Matsubara, M. Subramanian, A. Hayashi, Y. Hayashi, M. Tanemura, M. Kitazawa, R. Ohta, *Carbon* **2011**, *49*, 4191.
[37] Y. Liu, J. Zhang, H. Gao, Y. Wang, Q. Liu, S. Huang, C. F. Guo, Z. Ren, *Nano Lett.* **2017**, *17*, 1090.
[38] A. Chortos, Z. N. Bao, *Mater. Today* **2014**, *17*, 321.

